Defect modes in one-dimensional granular crystals

Y. Man,[1,2] N. Boechler,[1] G. Theocharis,[1] P. G. Kevrekidis,[3] and C. Daraio[1]
[1]*Graduate Aerospace Laboratories (GALCIT) California Institute of Technology, Pasadena, California 91125, USA*
[2]*Keble College, University of Oxford, Oxford OX1 3PG, UK*
[3]*Department of Mathematics and Statistics, University of Massachusetts, Amherst, Massachusetts 01003-4515, USA*
(Received 3 October 2011; published 29 March 2012)

We study the vibrational spectra of one-dimensional statically compressed granular crystals (arrays of elastic particles in contact) containing light-mass defects. We focus on the prototypical settings of one or two spherical defects (particles of smaller radii) interspersed in a chain of larger uniform spherical particles. We present a systematic measurement, using continuous noise, of the near-linear frequency spectrum within the spatial vicinity of the defect(s). Using this technique, we identify the frequencies of the localized defect modes as a function of the defect size and the position of the defects relative to each other. We also compare the experimentally determined frequencies with those obtained by numerical eigenanalysis and by analytical expressions based on few-site considerations. These approximate analytical expressions, based on normal-mode analysis, are found to be in excellent agreement with numerics for a wide range of mass ratios. We also observe that the experimentally measured frequencies of the localized defect modes are uniformly upshifted, compared to the numerically and theoretically predicted values.

DOI: 10.1103/PhysRevE.85.037601 PACS number(s): 63.20.Ry, 63.20.Pw, 45.70.−n, 46.40.−f

Introduction. Defect modes in crystals have long been studied in the realm of solid-state physics [1,2]. The presence of defects or "disorder" is known to enable localized lattice vibrations, whose associated frequencies have been measured in the spectra of real crystals (see Refs. [1,3] and references therein). More recently this study has been extended to superconductors [4] and electron-phonon interactions [5], among others. Similar phenomena have also been observed in nonlinear systems, including photonic crystals [6], optical waveguide arrays [7–9], dielectric superlattices (with embedded defect layers) [10], and micromechanical cantilever arrays [11].

Granular crystals are nonlinear systems composed of densely packed particles interacting through Hertzian contacts [12–15]. These systems present a remarkable ability to tune their dynamic response from linear to strongly nonlinear regimes [13]. This has allowed the exploration of nonlinear waveforms such as traveling waves [13–16] and discrete breathers [17]. Granular crystals have also been proposed for several engineering applications, such as energy absorbing layers [18–20], sound scramblers [21], and acoustic lenses [22] and rectifiers [23].

The presence of defects in statically uncompressed (or weakly compressed) granular chains excited by impulsive loading has been studied in a number of previous works that have reported the existence of dynamic responses such as the fragmentation of waves, anomalous reflections, and energy trapping [18–20,24–29]. In this paper we study the response of strongly compressed granular crystals, with one or two defects, excited by continuous signals. We measure the near-linear frequency response of the system and reveal localized modes due to the presence of defects. We report that the number of localized modes generically mirrors of the defects, and note that the frequencies of such modes depend on (1) the ratio of the defect mass to the mass of the particles in the uniform chain, (2) the relative proximity of multiple defects, (3) the geometric and material properties of the particles composing the crystal, and (4) the static load. Finally, we compare our experimental findings with numerical computations and with theoretical analysis approximating the behavior of a few sites in the vicinity of the defect(s) and analyzing the normal modes thereof.

Experimental setup. We assemble one-dimensional (1D) granular crystals, similar to those described in Refs. [17,30], composed of $N = 20$ statically compressed stainless steel spherical particles (316 type, with elastic modulus $E =$ 193 GPa and Poisson ratio $\nu_b = 0.3$ [31]), as shown in Fig. 1(a). The chain is composed of uniform particles of (measured) radius $R = 9.53$ mm and mass $M = 28.84$ g, except for one (or two) light-mass stainless-steel defect particles. The spheres are held in a 1D configuration using four polycarbonate bars (12.7 mm diameter) that are aligned by polycarbonate guide plates. The defect particles, which are of smaller radii than the rest of the particles of the chain, are aligned with the axis of the crystal using polycarbonate support rings. Dynamic perturbations are applied to the chain by a piezoelectric actuator (Piezomechanik PST 150/5/7 VS10) mounted on a steel cube (which acts as a rigid wall). The particles are statically compressed by a load of $F_0 = 20$ N. The static load is applied using a soft spring, of stiffness 1.24 kN/m, which is compressed between the last particle in the chain and a second steel cube bolted to the table. The applied static load is measured by a calibrated load cell placed between the spring and the steel cube. We measure the dynamic force signals of the propagating waves with custom-made force sensors consisting of a piezoelectric disk embedded inside two halves of a stainless steel particle with radius $R = 9.53$ mm. The sensor particles are carefully constructed to resemble the mass, shape, and contact properties of the other spherical particles [18,21,32,33].

Theoretical model. We consider the 1D inhomogeneous crystal of N beads as a chain of nonlinear oscillators [13]:

$$m_n\ddot{u}_n = A_n[\Delta_n + u_{n-1} - u_n]_+^p - A_{n+1}[\Delta_{n+1} + u_n - u_{n+1}]_+^p , \quad (1)$$

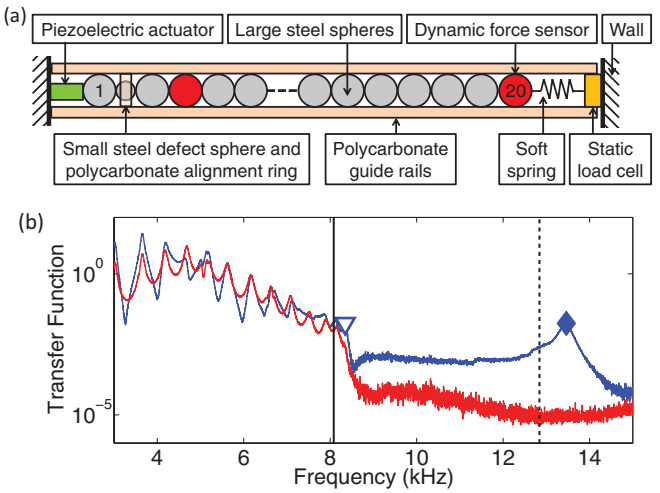

FIG. 1. (Color online) (a) Schematic diagram of the experimental setup for the homogeneous chain with a single-defect configuration. (b) Experimental transfer functions (as defined in the "single defect" section) for a granular crystal with a static load of $F_0 = 20$ N and a defect bead of mass $m = 5.73$ g located at site $n_{\text{def}} = 2$. Blue (dark gray) [red (light gray)] curves correspond to the transfer function obtained from the force signal of a sensor particle placed at $n = 4$ [$n = 20$]. The diamond marker is the identified defect mode. The triangle marker is the identified upper acoustic cutoff mode. The vertical black dashed (solid) line is the theoretically predicted defect-mode frequency (acoustic band cutoff frequency).

where $[Y]_+$ denotes the positive part of Y (which signifies that adjacent particles interact only when they are in contact), u_n is the displacement of the nth sphere (where $n \in \{1, \ldots, N\}$) around the static equilibrium, m_n is the mass of the nth particle, and the coefficients A_n depend on the exponent p and the geometry or material properties of adjacent beads. The exponent $p = 3/2$ represents the Hertz law potential between adjacent spheres [12]. In this case, $A_n = \frac{2E}{3(1-\nu^2)}\left(\frac{R_{n-1}R_n}{R_{n-1}+R_n}\right)^{1/2}$, and the static displacement obtained from a static load F_0 is $\Delta_n = (F_0/A_n)^{2/3}$ [12,13], where R_n is the radius of the nth particle.

In order to study the linear spectrum of the inhomogeneous granular crystal, we linearize Eq. (1) about the equilibrium state under the presence of the static load. This yields the following linear system [17,34,35]:

$$m_n\ddot{u}_n = K_n(u_{n-1} - u_n) - K_{n+1}(u_n - u_{n+1}), \tag{2}$$

where $K_n = \frac{3}{2}A_n^{2/3}F_0^{1/3}$. Following Ref. [34], we simplify Eq. (2) to the eigensystem:

$$-\omega^2\mathbf{M}\mathbf{u} = \Lambda\mathbf{u}, \tag{3}$$

where $\mathbf{M}$ is a $N \times N$ diagonal matrix with elements $M_{nn} = m_n$, and $\mathbf{u}$ is the displacement vector. $\mathbf{\Lambda}$ is a $N \times N$ tridiagonal matrix with elements $\Lambda_{mn} = -[K_n + (1 - \delta_{nN})K_{n+1}]\delta_{mn} + K_n\delta_{mn-1} + K_{n+1}\delta_{mn+1}$, where δ is the Kronecker delta and we consider left-fixed and right-free boundary conditions. We derive the right-free boundary assumption from the low stiffness of the static compression spring [Fig. 1(a)] as compared to the stiffness of the particles in contact.

Single defect. In this section, we study 1D granular crystals that are homogeneous except for one light-mass defect bead at site n_{def}, as shown in Fig. 1(a). The presence of the single light-mass defect generates a localized mode centered at the defect site, which we will refer to as the defect mode. The defect-mode amplitude decays exponentially away from the defect site, and its frequency f_d is such that $f_d > f_c$, where $f_c = \frac{1}{2\pi}\sqrt{\frac{4K_{RR}}{M}}$ is the upper cutoff frequency of the acoustic band of the homogeneous host crystal (where $K_{RR} = \frac{3}{2}A_{RR}^{2/3}F_0^{1/3}$ is the linear stiffness of the contact between two beads with radius R). The spatial profile of this mode consists of adjacent particles oscillating out of phase (see inset in Fig. 2). As the radius of the defect bead becomes smaller, the difference between f_d and f_c becomes larger, while the defect mode becomes more spatially localized [34]. We observe that for the granular crystals studied here, with radii ratios of $\frac{r}{R} < 0.7$, the defect mode involves the motion of up to approximately three beads, i.e., the displacements of the beads at $n \geqslant n_{\text{def}} + 2$ and $n \leqslant n_{\text{def}} - 2$ are negligible. Because in this range of radii ratio the motion of the particles can be accurately approximated by three beads, we consider the particles at $n = n_{\text{def}} \pm 2$ as fixed walls, in order to find an analytical approximation for the frequency of the defect mode. Solving for the eigenfrequencies of this reduced three-bead system, we find that the mode corresponding to the out of phase motion can be analytically approximated as the following:

$$f_{3\text{bead}} = \frac{1}{2\pi}\sqrt{\frac{2K_{Rr}M + K_{RR}m + K_{Rr}m + \sqrt{-8K_{Rr}K_{RR}mM + [2K_{Rr}M + (K_{RR} + K_{Rr})m]^2}}{2mM}}, \tag{4}$$

where $K_{Rr} = \frac{3}{2}A_{Rr}^{2/3}F_0^{1/3}$ is the linear stiffness of the contact between a defect bead and a bead of radius R, and m is the mass of the defect particle.

We conduct experiments to identify the frequency of the defect mode in granular crystals with a single light-mass defect as shown in Fig. 1(a). We place the defect particle at site $n_{\text{def}} = 2$ (close to the actuator) so that the energy applied by the actuator at the defect-mode frequency will not be completely attenuated by the uniform crystal (which acts as a mechanical frequency filter) before it arrives at the defect site. Because of the localized nature of the defect mode, placing a defect particle (of radius $r \leqslant 7.14$ mm) at site $n_{\text{def}} = 2$ or further into the chain makes nearly no difference on the frequency of the defect mode. For instance, for a defect particle of radius $r = 7.14$ mm, we numerically calculate [using Eq. (3)] the difference in the defect-mode frequency for the cases where

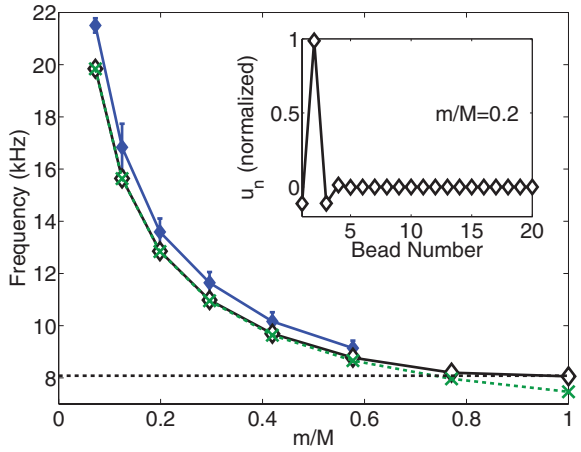

FIG. 2. (Color online) Frequency of the defect mode, with the defect bead placed at $n_{\text{def}} = 2$, as a function of mass ratio m/M. Solid blue line (dark gray, closed diamonds) corresponds to experiments, solid black line (open diamonds) to numerically obtained eigenfrequencies [see Eq. (3)], and green dashed line (light gray, x markers) to the analytical prediction of the three-bead approximation [see Eq. (4)]. The error bars account for statistical errors on the measured frequencies and are $\pm 2\sigma$. Inset: The normalized defect mode for $\frac{m}{M} = 0.2$.

a defect particle is placed at site $n_{\text{def}} = 2$ or $n_{\text{def}} = 10$, to be 3 Hz. Conversely, because of the presence of the fixed boundary and the larger localization length of the defect mode, for a defect particle of $r = 8.73$ mm, we calculate the difference in defect-mode frequency, between sites $n_{\text{def}} = 2$ and $n_{\text{def}} = 10$, to be 68 Hz. The defect particles are stainless-steel spheres of smaller radii, $r = [3.97,4.76,5.56,6.35,7.14,7.94]$ mm, and measured masses of $m = [2.08,3.60,5.73,8.54,12.09,16.65]$ g, respectively. We experimentally characterize the linear spectrum of this system by applying low-amplitude (approximately 200 mN) bandwidth-limited noise (3–25 kHz for the two smallest defect particles, and 3–15 kHz otherwise) via the piezoelectric actuator. We calculate the transfer functions, specific to the sensor location, by dividing the power spectral density (PSD) of the measured force-time history by the PSD of the input signal, and normalizing this ratio by its average level in the 3–8 kHz range (corresponding to the acoustic band). We embed sensors in particles at sites $n = 4$ and 20. In Fig. 1(b) we show the transfer functions for the granular crystal with defect radius $r = 5.56$ mm. We denote the experimentally measured acoustic band cutoff frequency by the triangular marker (found by identifying the last peak in the acoustic band) and defect-mode frequency as the diamond marker on the $n = 4$ transfer function. The vertical lines denote the theoretically determined upper cutoff frequency of the acoustic band and the defect frequency [Eq. (4)]. The presence of the defect mode can be clearly identified in the vicinity of the defect (at $n = 4$) but is not visible far from the defect (at $n = 20$).

We repeat the process of measuring the transfer function and identifying the defect-mode frequency 16 times, and reassemble the crystal after each repetition. In Fig. 2 we plot the average frequency of the 16 experimentally identified defect modes as a function of the mass ratio $\frac{m}{M}$ (blue [dark gray] solid line connecting the closed diamonds). We also plot, for comparison, the defect frequency predicted by the analytical expression of Eq. (4) (green [light gray] dashed line connecting the crosses), and the numerical eigenanalysis of Eq. (3) corresponding to the experimental setup (black solid line connecting the open diamonds). The error bars on the experimental data are $\pm 2\sigma$, where σ is the standard deviation of the identified defect frequencies over the 16 repetitions. Comparing the analytical three-bead approximation with the numerical eigenfrequencies, we find an excellent agreement for mass ratios of $\frac{m}{M} < 0.6$. Comparing the experimental data with the numerics, we find an upshift of 5%–10%, similar to the upshift observed in Refs. [17,30]. For the $r = 5.56$ mm defect, the average experimental defect-mode frequency is $f_d^{\text{exp}} = 13.59$ kHz, and the average experimental cutoff frequency is $f_c^{\text{exp}} = 8.36$ kHz. In comparison, the theoretical three-bead approximation gives a defect-mode frequency of $f_d^{\text{3bead}} = 12.84$ kHz and the eigenproblem of Eq. (3) gives a defect-mode frequency of $f_d^{\text{num}} = 12.85$ kHz, while the analytically calculated cutoff frequency was $f_c = 8.02$ kHz.

Possible reasons for these upshifts have been identified in Refs. [17,30] and the references therein, such as error in the material parameters, nonlinear elasticity, surface roughness, dissipative mechanisms, and misalignment of the particles. Nevertheless, it is clear from Fig. 2 that the functional dependence of the relevant frequencies on the mass ratio (of defect to regular beads) is accurately captured by our analytical and numerical results.

Two defects. We study granular crystal configurations with two identical light-mass defects to better understand the effects of increasing heterogeneity on the spectral response of the system. We can expect that two light-mass defects placed far from each other in a granular crystal (sufficiently outside this localization length) would have similar frequencies and mode shapes that are independent of the presence of the other defect. However, as the two defect particles are brought closer together (within the localization length), each mode influences the other. This results in the creation of two defect modes at different frequencies: one with the defect particles moving out of phase, and the other with the defect particles moving in phase. For the case of nearest-neighbor identical defects, our theoretical analysis can be extended by using a four-particle analogy. In this case, using the notation $s_1 = K_{Rr}(M+m) + K_{RR}m$, $s_2 = -4K_{Rr}K_{RR}Mm + [K_{RR}m + K_{Rr}(M+m)]^2$, $s_3 = s_1 + 2K_{rr}M$ and $s_4 = -4[2K_{rr}K_{RR} + K_{Rr}(2K_{rr} + K_{RR})]Mm + [2K_{rr}M + K_{RR}m + K_{Rr}(M+m)]^2$, we obtain the following frequencies:

$$f_{4\text{bead}}^{(1)} = \frac{1}{2\pi}\sqrt{\frac{1}{2Mm}(s_1 \pm \sqrt{s_2})}, \tag{5}$$

$$f_{4\text{bead}}^{(2)} = \frac{1}{2\pi}\sqrt{\frac{1}{2Mm}(s_3 \pm \sqrt{s_4})}. \tag{6}$$

The two highest frequencies correspond to the linear defect-mode frequencies. Naturally, this analytical approach can be extended to more distant defects, although we do not present such algebraically intensive cases here.

In Fig. 3 we show the behavior of two $r = 5.56$ mm defects in a $N = 20$ particle granular crystal under $F_0 = 20$ N static load, where the first defect is at site $k = n_{\text{def1}} = 2$ and the second defect is at a variable position between site $l = n_{\text{def2}} = 3$ and $l = n_{\text{def2}} = 6$. We use the same experimental method

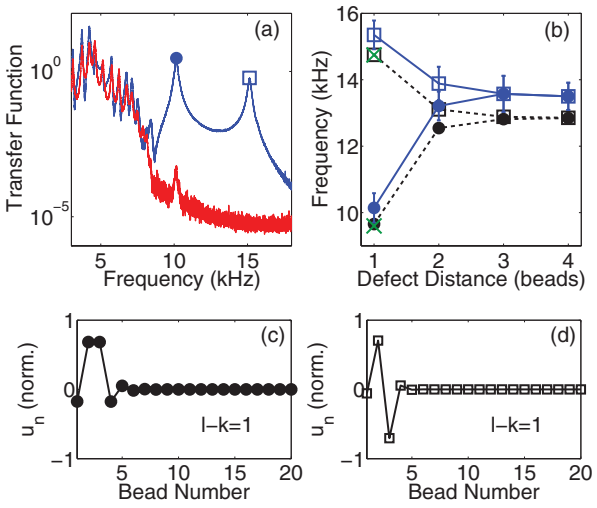

FIG. 3. (Color online) (a) Experimental transfer functions for a granular crystal with two defect beads of mass ratio $\frac{m}{M} = 0.2$ located at $n_{\text{def}} = 2$ and $n_{\text{def}} = 3$ (in contact). The blue (dark gray) [red (light gray)] curve corresponds to the transfer function obtained from the force signal of a sensor placed at $n = 4$ [$n = 20$]. (b) Frequencies of the defect modes as a function of the distance between them. The solid line denotes experimental data, the dashed line the numerically obtained eigenfrequncies, and the x markers the frequencies from the analytical expressions of Eqs. (5) and (6). (c, d) The normalized defect-mode shapes corresponding to the defect modes identified in (a) with frequency of the same marker type.

as in the single-defect case except now we use a noise range between 3–20 kHz and we place the first sensor at $n = l + 1$. We show the experimentally determined PSD transfer function for the case of $l - k = 1$ in Fig. 3(a), with sensors at site $n = 4$ (blue [dark gray]) and $n = 20$ (red [light gray]). As described in Ref. [34], the existence of two separate defect modes, for the case where the defect particles are adjacent to each other ($l - k = 1$), depends on the mass ratio of the defect particles to those of the rest of the crystal. Here the mass ratio is such that two modes are present, as can be seen in the blue (dark gray) curve in Fig. 3(a). The two distinct modes, which we denote by the open square and closed circular markers, have frequencies above the acoustic band. The square markers denote the mode with defect beads moving out of phase, and the closed circular marker corresponds to the mode with defect particles moving in phase, as shown by the numerically calculated eigenmodes in Fig. 3(c) and 3(d), respectively [34]. In Fig. 3(b), we plot the experimentally determined frequencies of both modes as a function of the interdefect particle distance ($l - k$). The solid blue (dark gray) lines are the experimental data, and the dashed black lines are the frequencies obtained from solving the eigenvalue problem of Eq. (3). The green (light gray) x markers denote the frequencies calculated with Eqs. (5) and (6), for the $l - k = 1$ case. It is evident that the analytical results agree closely with the numerically calculated eigenfrequencies. We see close qualitative agreement between the experimental data and the numerical predictions, but also the same systematic upshift as observed in the single-defect case and [17,30]. From Fig. 3(b), we can see that as the defects are placed three or more particles apart, the frequencies of the defect modes converged to approximately the same value, which suggests that the defects respond independently of each other.

Conclusions. We studied the response of statically compressed granular crystals containing light-mass defects. We made a systematic measurement of their near-linear spectra using continuous noise excitation. We demonstrated that such chains support localized modes with frequencies above that of their acoustic band cutoff, using approximate few-bead analytical calculations, numerics, and experiments. We observed a uniform upshift of the experimentally determined defect-mode frequencies, as compared to the numerically and theoretically predicted values, and offered a number of plausible causes of this feature. The analytical expressions are based on a normal mode analysis of a few-bead system. We should highlight here that a distinctive feature of a linear granular lattice is that the presence of one or more impurities induces mass and stiffness defects at the same time (as opposed to the more commonly tackled case of, e.g., purely mass defects). Furthermore, analogous arguments to the ones presented herein could be followed and applied to other branches of physics including phononic and photonic crystals, especially so in the less frequently tackled case of multiple defects. We also described how the number of supported localized modes depends on the number of defects, while their frequencies depend on the interdefect distance, on the ratio $\frac{m}{M}$ of defect to regular masses (and the geometric or elastic properties of the beads), and on the static load. This study furthers our understanding of the interplay of disorder and discreteness in discrete systems and provides an important framework for future studies of the nonlinear dynamics of granular crystals containing defects, and its reported results may be directly relevant to the design of granular crystals for applications involving vibrational energy trapping.

Acknowledgment. We thank Stéphane Job for help with the experimental setup. G.T. and P.G.K. acknowledge support from the A.S. Onassis Public Benefit Foundation through RZG 003/2010-2011 and PGK also through NSF-CMMI-1000337. C.D. acknowledges support from NSF-CMMI-969541 and NSF-CMMI-844540 (CAREER).

[1] A. A. Maradudin, E. W. Montroll, and G. H. Weiss, *Theory of Lattice Dynamics in the Harmonic Approximation* (Academic, New York, 1963).

[2] I. M. Lifschitz, Nuovo Cimento Suppl. **3**, 716 (1956); I. M. Lifschitz and A. M. Kosevich, Rep. Prog. Phys. **29**, 217 (1966).

[3] G. Lucovsky, M. H. Brodsky, and E. Burstein, Phys. Rev. B **2**, 3295 (1970).

[4] A. F. Andreev, JETP Lett. **46**, 584 (1987); A. V. Balatsky, Nature (London) **403**, 717 (2000).

[5] M. I. Molina and G. P. Tsironis, Phys. Rev. B **47**, 15330 (1993); G. P. Tsironis, M. I. Molina, and D. Hennig, Phys. Rev. E **50**, 2365 (1994).

[6] S. Y. Jin *et al.*, Science **282**, 274 (1998); M. G. Khazhinsky and A. R. McGurn, Phys. Lett. A **237**, 175 (1998).

[7] U. Peschel *et al*., Appl. Phys. Lett. **75**, 1348 (1999).
[8] R. Morandotti *et al*., Opt. Lett. **28**, 834 (2003).
[9] E. Smirnov *et al*., Opt. Express **14**, 11248 (2006).
[10] E. Lidorikis, K. Busch, Q. Li, C. T. Chan, and C. M. Soukoulis, Phys. Rev. B **56**, 15090 (1997).
[11] M. Sato *et al*., Europhys. Lett. **66**, 318 (2004).
[12] K. L. Johnson, *Contact Mechanics* (Cambridge University Press, Cambridge, 1985).
[13] V. F. Nesterenko, *Dynamics of Heterogeneous Materials* (Springer, New York, 2001).
[14] S. Sen *et al*., Phys. Rep. **462**, 21 (2008).
[15] C. Coste, E. Falcon, and S. Fauve, Phys. Rev. E **56**, 6104 (1997).
[16] M. A. Porter, C. Daraio, E. B. Herbold, I. Szelengowicz, and P. G. Kevrekidis, Phys. Rev. E **77**, 015601(R) (2008).
[17] N. Boechler *et al*., Phys. Rev. Lett. **104**, 244302 (2010); G. Theocharis, N. Boechler, P. G. Kevrekidis, S. Job, M. A. Porter, and C. Daraio, Phys. Rev. E **82**, 056604 (2010).
[18] C. Daraio, V. F. Nesterenko, E. B. Herbold, and S. Jin, Phys. Rev. Lett. **96**, 058002 (2006).
[19] J. Hong, Phys. Rev. Lett. **94**, 108001 (2005).
[20] R. Doney and S. Sen, Phys. Rev. Lett. **97**, 155502 (2006).
[21] V. F. Nesterenko, C. Daraio, E. B. Herbold, and S. Jin, Phys. Rev. Lett. **95**, 158702 (2005).
[22] A. Spadoni and C. Daraio, Proc. Natl. Acad. Sci. USA **107**, 7230 (2010).
[23] N. Boechler, G. Theocharis, and C. Daraio, Nat. Mater. **10**, 665 (2011).
[24] E. Hascoet and H. J. Hermann, Eur. Phys. J. B **14**, 183 (2000).
[25] E. J. Hinch and S. Saint-Jean, Proc. R. Soc. London A **455**, 3201 (1999).
[26] J. B. Hong and A. G. Xu, Appl. Phys. Lett. **81**, 4868 (2002).
[27] S. Sen, M. Manciu, and J. D. Wright, Phys. Rev. E **57**, 2386 (1998).
[28] M. Manciu, S. Sen, and A. J. Hurd, Physica A **274**, 588 (1999); **274**, 607 (1999).
[29] S. Job, F. Santibanez, F. Tapia, and F. Melo, Phys. Rev. E **80**, 025602(R) (2009).
[30] N. Boechler *et al*. J. Appl. Phys. **109**, 074906 (2011).
[31] *Metals Handbook*, 10th ed. (ASM International, Materials Park, OH, 1990).
[32] S. Job, F. Melo, A. Sokolow, and S. Sen, Phys. Rev. Lett. **94**, 178002 (2005).
[33] V. F. Nesterenko, A. N. Lazaridi, and E. B. Sibiryakov, Prikl. Mekh. Tekh. Fiz. **2**, 19 (1995).
[34] G. Theocharis *et al*., Phys. Rev. E **80**, 066601 (2009).
[35] E. B. Herbold *et al*., Acta Mech. **205**, 85 (2009).